analytical chemistry

ACS AuthorChoice

Article

pubs.acs.org/ac

Terms of Use

Coupling Isotachophoresis with Affinity Chromatography for Rapid and Selective Purification with High Column Utilization, Part 1: Theory

Viktor Shkolnikov and Juan G. Santiago*

Department of Mechanical Engineering, Stanford University, Stanford, California 94305, United States

Supporting Information

ABSTRACT: We present a novel technique that couples isotachophoresis (ITP) with affinity chromatography (AC) to achieve rapid, selective purification with high column utilization. ITP simultaneously preconcentrates an analyte and purifies it, based on differences in mobility of sample components, excluding species that may foul or compete with the target at the affinity substrate. ITP preconcentration accelerates the affinity reaction, reducing assay time, improving column utilization, and allowing for capture of targets with higher dissociation constants. Furthermore, ITP-AC separates the target and contaminants into nondiffusing zones, thus achieving high resolution in a short distance and time. We present an analytical model for spatiotemporal dynamics of ITP-AC. We identify and explore the effect of key process parameters, including target distribution width and height, ITP zone velocity, forward and reverse reaction constants, and probe concentration on necessary affinity region length, assay time, and capture efficiency. Our analytical approach shows collapse of these variables to three nondimensional parameters. The analysis yields simple analytical relations for capture length and capture time in relevant ITP-AC regimes, and it demonstrates how ITP greatly reduces assay time and improves column utilization. In the second part of this two-part series, we will present experimental validation of our model and demonstrate ITP-AC separation of the target from 10,000-fold more-abundant contaminants.

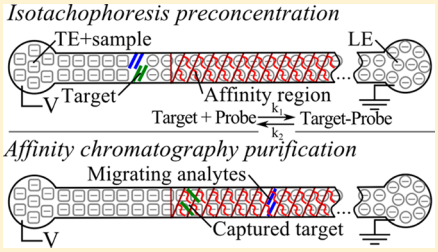

Affinity chromatography (AC) is a chromatographic technique that leverages a specific binding agent—the affinity ligand—for purification, separation, and/or analysis of sample components. The affinity ligand (probe) is used to selectively yet reversibly capture the sample component of interest (target). Numerous samples and sample components have been and continue to be analyzed or purified using AC, including enzymes, lectins, other proteins, and nucleic acids.[1−4] For many samples, including important biological samples (e.g., blood, cell lysate), the component of interest is present in very low concentration, while background, potentially fouling species are present in relatively high concentrations. This necessitates processing of a substantial sample volume through the affinity substrate. In addition, low target concentrations imply low target-probe binding rates.[5] These factors each increase the time of the affinity assay, can lead to poor substrate utilization, and/or poor purification yield, limiting applications of the method.

The aforementioned limitations of AC can be addressed by increasing the forward binding rate constant of reactions,[5] but the binding rate constant is often difficult to improve upon.[2] A second method is to preconcentrate and purify the target prior to the affinity reaction. Here, we explore the effect of increasing target purity and concentration using isotachophoresis (ITP). ITP uses a buffer with a high mobility co-ion (same charge as the analyte) and a second buffer with a co-ion that has lower mobility. Analyte species of intermediate mobility focus between these co-ions and are thereby preconcentrated and separated.[6,7] ITP has been demonstrated in a variety of applications related to the current work, including extraction and purification of nucleic acids from complex biological samples,[8] and 14 000-fold acceleration of homogeneous nucleic acid hybridization reactions in free solution.[9]

ITP has been used in conjunction with affinity assays in several applications, and several models for these processes have been developed. For example, Garcia-Schwartz et al. presented an approach combining ITP and an affinity reaction to detect micro-RNA.[10,11] They used ITP to accelerate hybridization between a mobile target species and a mobile fluorescent DNA probe in a microchannel. This ITP zone was then transported into a channel section containing cross-linked polyacrylamide gel functionalized with DNA complementary to the fluorescent DNA probe. This method was used to remove signal background (a negative enrichment strategy) and, therefore, enhance quantitation and specificity.[10,11] Garcia-Schwartz et al. presented a volume-averaged model for the reaction of the mobile species. However, their analysis did not treat the spatiotemporal dynamics of the surface (gel) affinity reaction. Their analysis focuses on reactions prior to and after the affinity column and assumes that the affinity capture occurs instantaneously in negligible space. Recently (work published during preparation of this manuscript), Karsenty et al. used ITP

Received: March 27, 2014
Accepted: May 31, 2014
Published: June 17, 2014

   dx.doi.org/10.1021/ac5011052 | *Anal. Chem.* 2014, 86, 6220−6228

to accelerate a reaction of a DNA target to an immobilized DNA probe on a short region of stationary magnetic beads and present a model for this process.[12] Their model captures the temporal, volume-averaged dynamics of a reaction between a target preconcentrated with ITP and a bead immobilized probe. However, their model only addresses the regime where the target concentration remains approximately constant during the reaction and is only applicable to short (order of ITP peak width) capture regions. Their model does not address the spatial dynamics of the reaction. Despite these related studies, we know of no model or analysis of the coupled spatiotemporal dynamics of a reaction between a species focused in ITP and a surface, gel, or porous region.

Here, we investigate the theory behind physicochemical processes of integrating ITP and AC. We consider the case of an AC column composed of a porous polymer monolith (PPM) functionalized with a synthetic cDNA ligand. However, the current approach is easily extended to any integration of ITP and a stationary affinity column. The goal of this type of integration is to (a) drastically reduce assay time; (b) improve column utilization; (c) allow for capture of targets with higher dissociation constants; (d) obviate the need for high-pressure specialized pumps; (e) directly integrate an automatic wash step into the process, eliminating a separate wash step; and (f) reduce affinity substrate fouling (and competing reactions) by partially separating sample compounds by their electrophoretic mobility.

We describe the principle of coupling ITP preconcentration and AC purification. We derive and present an analytically solvable one-dimensional transport model for coupling of ITP with a semi-infinite AC porous column and second-order reversible reaction kinetics. Our model describes the spatiotemporal dynamics of target-probe binding in the affinity region, allowing for complete capture of the target. This includes the coupled effects of target distribution width, distribution intensity, ITP zone velocity, forward and reverse reaction constants, and probe concentration on necessary affinity region length, assay time, and capture efficiency. Our new analytical approach allows us to collapse these six independent variables down to three nondimensionalized parameters summarizing all regimes. In the second part of this two-paper series,[13] we experimentally validate our model and demonstrate sequence specific purification of 25 nt target DNA from 10 000-fold more-abundant fish sperm DNA.

CONCEPT AND THEORY

Method Concept. We aimed to decrease the assay time and improve affinity region utilization by purifying the target and increasing the affinity capture reaction rate. Figure 1 summarizes the key aspects of our approach and the initial conditions for our model. As in the experiments we will show in the second part of this two-paper series, we consider a free-standing capillary that contains a porous affinity region. The affinity region contains pores sufficiently large to allow easy pressure-driven pumping of liquid or air. First, we fill leading electrolyte (LE) in the LE reservoir and in the entire capillary (including the porous affinity region). We then fill the trailing electrolyte (TE) reservoir with a mixture of trailing electrolyte buffer and sample. Upon application of the electric field, the target is extracted from the TE reservoir, preconcentrated into the LE/TE interface, and transported toward and through the affinity region (Figure 1a). Possible contaminating species that are neutral, oppositely charged of the target, or co-ionic but

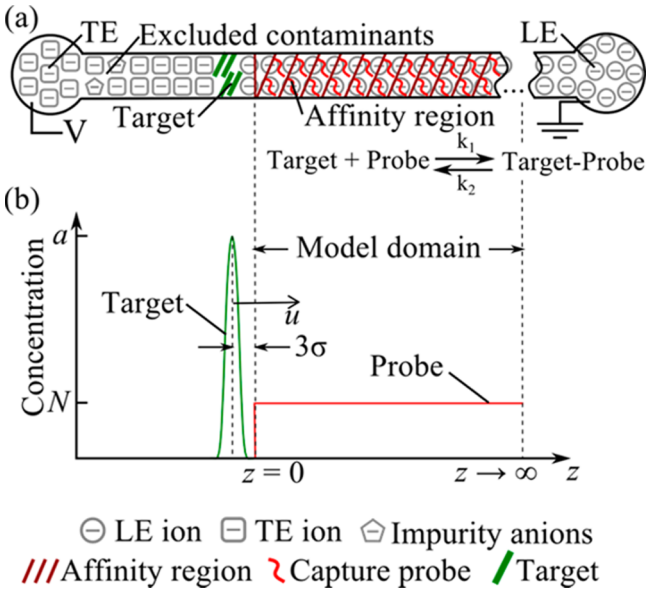

Figure 1. (a) Schematic of assay for ITP-aided affinity chromatography (ITP-AC). We consider an assay in a capillary with a semi-infinite affinity capture region as shown. Under the influence of an electric field, the target is extracted from a sample reservoir, separated from contaminants, and concentrated at the LE/TE interface. It is then transported to and through the affinity region. Within the affinity region, the target reacts with the immobilized capture probe via a second-order reversible reaction where k_1 and k_2 are the forward and reverse reaction rate constants, respectively. (b) Initial conditions for our model of ITP-AC. At $t = 0$, the target has a Gaussian distribution with standard deviation σ and peak concentration a; its peak is located 3σ from the entrance of the affinity region. The target moves with velocity u through the affinity region. The affinity region is semi-infinite beginning at $z = 0$ (where z is the axial coordinate of the capillary) and containing a uniformly distributed probe of volume-averaged concentration N.

with a lower electrophoretic mobility magnitude than the TE co-ion are excluded.[8] Upon reaching the affinity region, the target reacts with the immobilized capture probe and is captured. After capture, we pump air through the system to remove all liquid from the column and therefore arrest further reactions.

The initial focusing of ITP is selective[6,8] and helps prevent fouling of the affinity region by unfocused background species. The increase of the target concentration via ITP promotes faster capture reaction and the target is captured in a smaller, upstream region of the column. Exposure of the ITP-focused analyte to reaction sites on the column is temporary and is followed by a wash associated with the TE zone entering the column. We limit the time between this electrokinetic wash step and the removal of liquids with air to control the stringency of the wash step. This approach limits the time for dissociation reaction to occur so the captured target concentration is effectively "frozen" by the introduction of air. This enables capture of targets with relatively high dissociation rate, if necessary.

Transport and Focusing of Trace Analytes in Isotachophoresis. ITP is an electrokinetic technique used to preconcentrate and separate analytes.[6,7,14] Here, we leverage a mode of ITP known as "peak mode" ITP, where trace analytes co-focus into a relatively narrow peak at the interface of LE and TE.[14−16] In peak mode ITP, trace analytes do not

dx.doi.org/10.1021/ac5011052 | Anal. Chem. 2014, 86, 6220−6228

appreciably contribute to local conductivity. The peak width and analyte locations are determined by the mobilities of the ions of LE and TE and electric fields established by and at the interface between TE and LE buffers.[16] The analyte mobility in the TE zone is higher than that of the TE co-ion. The analyte mobility in the LE zone is also lower than that of the LE co-ion. This arrangement of mobilities enables purification of, for example, nucleic acids from complex mixtures and excludes possible fouling species from the ITP zone.[8,14] If, as in our case, the analyte mobility is significantly different from that of the LE and TE ions, the target distribution is narrow and approximately Gaussian in shape.[16]

One-Dimensional Transport Reaction Model. We derive an unsteady, one-dimensional model for ITP which we will show captures the essential dynamics of the process. We chose a reduced-order model to identify the key governing parameters of the process. We model focusing of an ionic target in peak mode ITP, and migrating toward a semi-infinite affinity capture region. In the affinity region, the target reacts with the surface bound probe according to a simple second-order reversible reaction of the following form: Target + Probe $\rightleftharpoons$ Target − Probe. We set time $t = 0$ at the point where the target just starts to enter the affinity region (Figure 1b). We assume that the target has a Gaussian concentration profile with a width given by the interface width between the LE and the TE. This is a common assumption for modeling the distribution of trace analyte focused at the LE/TE interface.[9,15,17] As usual for peak mode ITP, we further assume that the change in concentration of the target has no effect on the electric field in ITP.[9,15,17] We start with the general advection-diffusion equation for the solution inside the porous affinity region with second-order reversible reaction at the surface:

$$\frac{\partial c'}{\partial t} = \nabla\cdot(D\nabla c') - \nabla\cdot(\vec{u}c') \tag{1}$$

where c' is the local target concentration, $\vec{u}$ the target velocity, D the target diffusion coefficient, and t time. The reaction with the target occurs at the boundary between the solvent and the surfaces of the porous solid. The solid is impermeable to the target and fluid. Hence, at this boundary, we have

$$-D\nabla c'\cdot\vec{q} = k_1'c'(N' - n') - k_2'n' \tag{2}$$

where $\vec{q}$ is the unit normal to the surface of the monolith, n' is the surface density of the captured target (moles per area), N' is the initial surface density of the probe, and k_1' and k_2' are the forward and reverse constants, respectively. We also have an auxiliary relation for n':

$$\frac{\partial n'}{\partial t} = -k_1'c'(N' - n') + k_2'n' \tag{3}$$

To simplify these three-dimensional (3D) equations, we note that the net flow occurs along the direction of the axis of the macroscopic porous affinity region and that this region is homogeneous and anisotropic. We model the region as a bundle of tortuous cylindrical pores[18] with a mean tortuosity τ. We define a coordinate s that follows the center contour of these tortuous cylindrical pores, the coordinate r that is locally normal to s, and the azimuthal θ for cylindrical coordinates. We also note that we assume the target diffusion coefficient D to be constant everywhere. Therefore, we rewrite eqs 1 and 2 as

$$\frac{\partial c'}{\partial t} = D\left[\frac{1}{r}\frac{\partial}{\partial r}\left(r\frac{\partial c'}{\partial r}\right) + \frac{1}{r^2}\frac{\partial^2 c'}{\partial\theta^2} + \frac{\partial^2 c'}{\partial s^2}\right] - \left[\frac{1}{r}\frac{\partial(ru_r c')}{\partial r} + \frac{1}{r}\frac{\partial(u_\theta c')}{\partial\theta} + \frac{\partial(u_s c')}{\partial s}\right] \tag{4}$$

$$-D\frac{\partial c'}{\partial r}\bigg|_{r=r_0} = k_1'c'(N' - n') - k_2'n' \tag{5}$$

where r_0 is the radius of the pore. We assume that inside the tortuous pore the fluid flows only in the axial direction, and, hence, $u_r = u_\theta = 0$. This simplifies eq 4 to

$$\frac{\partial c'}{\partial t} = D\left[\frac{1}{r}\frac{\partial}{\partial r}\left(r\frac{\partial c'}{\partial r}\right) + \frac{1}{r^2}\frac{\partial^2 c'}{\partial\theta^2} + \frac{\partial^2 c'}{\partial s^2}\right] - \frac{\partial(u_s c')}{\partial s} \tag{6}$$

Next, we consider the rates of diffusion from the bulk of a pore to the pore surface where the reaction takes place, and the rate of reaction. The time for the target to diffuse from the center of the pore to the pore surface scales as[19]

$$t_{\text{diff}} \approx \frac{{r_0}^2}{D} \tag{7}$$

and the time for the target to be captured scales as

$$t_{\text{rxn}} \approx \frac{1}{k_1 N} \tag{8}$$

We take the diffusion coefficient of our target DNA oligomer to be roughly 10^{-6} cm^2 s^{-1}. This is a typical magnitude of the diffusion coefficient for 20 nt oligomers in aqueous solution.[20] Using this, and the forward rate constant, the probe density, and the pore size that we obtained in this work (see Part 2 of this two-part series[13]), we find $t_{\text{diff}} \approx 10^{-6}$ s and $t_{\text{rxn}} \approx 20$ s. We conclude that the pore remains locally well mixed via diffusion, despite the reaction, yielding an approximately uniform concentration through the microscale tortuous pore cross-sectional area. Therefore, we simplify eqs 6 and 5 further by defining the averaged concentration based on the pore cross-sectional area:

$$c''(s) \equiv \frac{1}{\pi r_0^2}\int_0^{r_0}\int_0^{2\pi} c'(r,\theta,s)r\,\mathrm{d}r\,\mathrm{d}\theta \tag{9}$$

We then integrate eq 6, subject to the boundary condition desribed by eq 5 over r from 0 to r_0 and over θ from 0 to 2π and obtain

$$\frac{\partial c''}{\partial t} + \frac{\partial(u_s c'')}{\partial s} = D\frac{\partial^2 c''}{\partial s^2} - k_1''c''(N'' - n'') + k_2''n'' \tag{10}$$

$$\frac{\partial n''}{\partial t} = -k_1''c''(N'' - n'') + k_2''n'' \tag{11}$$

Next, we transform eq 10 into the axial coordinate of the porous monolith, z (which is along the major axis of monolith and capillary, see Figure 1). As is usual, the coordinate z is related to the pore coordinate s through tortuosity τ such that $\tau = s/z$.

$$\frac{\partial c''}{\partial t} + \frac{1}{\tau}\frac{\partial(u_s c'')}{\partial z} = D\frac{1}{\tau^2}\frac{\partial^2 c''}{\partial z^2} - k_1''c''(N'' - n'') + k_2''n'' \tag{12}$$

dx.doi.org/10.1021/ac5011052 | Anal. Chem. 2014, 86, 6220−6228

Next, we define an effective concentration averaged over the cross-sectional area for the monolith as

$$c = \frac{1}{A_M}\int_{A_M} c_i'' \, dA = \frac{A_{cap}}{A_M}\frac{1}{M}\sum_{i=1}^{M} c_i'' \tag{13}$$

where A_M is the geometric cross-sectional area of the monolith, A_{cap} the total cross-sectional area of the pores, and M the total number of the tortuous cylindrical pores making up the monolith. We define the void fraction (φ) to be $\varphi = A_{cap}/A_M$. We apply this average to all tortuous cylindrical pores in the tortuous pore bundle concentration, which is described by eqs 12 and 11 to obtain

$$\frac{\partial c}{\partial t} + \frac{\partial (vc)}{\partial z} = D\frac{1}{\tau^2}\frac{\partial^2 c}{\partial z^2} - k_1 c(N - n) + k_2 n \tag{14}$$

$$\frac{\partial n}{\partial t} = -k_1 c(N - n) + k_2 n \tag{15}$$

where v is the superficial velocity.[18] We henceforth work with this concentration as it directly defines the capacity of the affinity region (i.e., moles of target that can be captured per geometric volume of affinity region) and is directly, experimentally observable.

We simplify eq 14 by expanding the target velocity into a uniform velocity, u (i.e., not a function of z), and a perturbation $\tilde{u}$, which depends on z and t as follows:

$$v(z) = u + \tilde{u}(z, t) \tag{16}$$

The expansion of eq 14 follows:

$$\frac{\partial c}{\partial t} + u\frac{\partial c}{\partial z} + \frac{\partial (\tilde{u}c)}{\partial z} = D\frac{1}{\tau^2}\frac{\partial^2 c}{\partial z^2} - k_1 c(N - n) + k_2 n \tag{17}$$

For our process, we assume our target remains focused by ITP, so that its velocity v is governed by the electric field of the ITP near the LE/TE interface.[6] Our experimental observations confirm that this assumption is accurate for the cases we considered (e.g., where the target has strong affinity for the immobilized probe). Experimentally, we observe zones of unbound analytes remain focused in ITP and traveling at ITP-controlled velocities, despite potential reactions with the affinity column (see the second part of this two-part series[13]). We note that, for situations where pressure-driven and electro-osmotic flow are important, we hypothesize that we can assume the advection velocity of the LE/TE interface will be the arithmetic sum of the macroscopic ITP and bulk flow velocities through the column. Next, we use this empirical observation concerning analyte velocity to construct an approximate (heuristic) description of the analyte velocity distribution near the ITP zone interface.

The target is a trace analyte, so it does not contribute significantly to the conductivities of the zones and, hence, the local electric field.[9,15,17] Hence, for a trace analyte focused at the LE/TE interface, its velocity is governed by the electric field distribution near the TE-to-LE interface. This shape of the electric field distribution can be approximated as a sigmoidal curve, being highest in the TE and lowest in the LE.[6,21] Here, we approximate the electric field as an error function. Furthermore, the LE/TE interface electromigrates at the ITP zone velocity, so we assume that the inflection of the sigmoid also migrates with the LE/TE interface. We let the deviation of the target velocity from the ITP LE/TE interface velocity u be some small fraction of the LE-TE velocity (εu). We set the characteristic width of the LE/TE interface as σ. Hence, we express the target velocity as

$$v = u + \varepsilon u \,\mathrm{erf}\left[-\frac{(z - ut + 3\sigma)}{\sigma}\right] \tag{18}$$

which has the form of a uniform velocity plus a perturbation, as in eq 16. We approximate the quantity εu, the amplitude of the error function, as the difference between the analyte velocity in the adjusted TE (equal to $\mu_{a,TE}E_{TE}$, where E_{TE} is the electric field in the TE) and that the ITP LE/TE interface (equal to $\mu_{TE\ ion,TE}E_{TE}$[6]). Therefore, we write the smallness parameter as simply

$$\varepsilon = \frac{\mu_{a,TE} - \mu_{TE\ ion,TE}}{\mu_{TE\ ion,TE}} \tag{19}$$

$\mu_{a,TE}$ is the mobility of the analyte in the TE, and $\mu_{TE\ ion,TE}$ is the mobility of the TE ion in the TE. To exclude many contaminating species from focusing with the analyte, we choose the TE ion mobility to be near to that of the analyte (for example, within 10%−20%), which makes ε small.

Next we cast eqs 17 and 15 in dimensionless form as follows: c^* and n^* are free-target and bound-target concentrations normalized by initial probe concentration N; t^* is the time normalized by the reaction time scale $1/(k_1N)$ and z^* is the axial coordinate normalized by the advection-reaction length scale $u/(k_1N)$; and β is the nondimensionalized equilibrium dissociation constant ($\beta = k_2/(k_1N)$). We scale $\tilde{u}$ by εu for $\tilde{u}^*$. We obtain

$$\frac{\partial c^*}{\partial t^*} + \frac{\partial c^*}{\partial z^*} + \varepsilon\frac{\partial (\tilde{u}^* c^*)}{\partial z^*} = \frac{Dk_1N}{\tau^2 u^2}\frac{\partial^2 c^*}{\partial z^{*2}} - c^*(1 - n^*) + \beta n^* \tag{20}$$

$$\frac{\partial n^*}{\partial t^*} - c^*(1 - n^*) + \beta n^* = 0 \tag{21}$$

As we shall show in Part 2 of this two-part series,[13] our process is well-characterized by the following parameters: $D \approx 10^{-6}$ cm^2 s^{-1},[20] $k_1 \approx 10^3$ M^{-1} s^{-1}, $N \approx 30$ μM, $u \approx 0.05$ mm s^{-1}, and τ = 1−2. We therefore estimate $Dk_1N/(\tau^2u^2)$ to be between 0.0003 and 0.001, significantly smaller than unity. We thus drop the first term on the right-hand side and simplify eq 20 to

$$\frac{\partial c^*}{\partial t^*} + \frac{\partial c^*}{\partial z^*} + \varepsilon\frac{\partial (\tilde{u}^* c^*)}{\partial z^*} + c^*(1 - n^*) - \beta n^* = 0 \tag{22}$$

We combine eqs 22 and 21 as

$$\frac{\partial c^*}{\partial t^*} + \frac{\partial c^*}{\partial z^*} + \varepsilon\frac{\partial (\tilde{u}^* c^*)}{\partial z^*} + \frac{\partial n^*}{\partial t^*} = 0 \tag{23}$$

$$\frac{\partial n^*}{\partial t^*} - c^*(1 - n^*) + \beta n^* = 0 \tag{24}$$

We seek a straightforward expansion for the solution of eqs 23 and 24 in the form $c = c_0 + \varepsilon c_1 + \varepsilon^2 c_2{}^2 + \ldots$, and $n = n_0 + \varepsilon n_1 + \varepsilon^2 n_2{}^2 + \ldots$. Then substitute these into eqs 23 and 24. Collecting the coefficients of each power of ε and equating:

dx.doi.org/10.1021/ac5011052 | Anal. Chem. 2014, 86, 6220−6228

ε^0:

$$\frac{\partial c_0^*}{\partial t^*} + \frac{\partial c_0^*}{\partial z^*} + \frac{\partial n_0^*}{\partial t^*} = 0$$
$$\frac{\partial n_0^*}{\partial t^*} - c_0^*(1 - n_0^*) + \beta n_0^* = 0 \quad (25)$$

ε^1:

$$\frac{\partial c_1^*}{\partial t^*} + \frac{\partial c_1^*}{\partial z^*} + \frac{\partial n_1^*}{\partial t^*} + \frac{\partial(\tilde{u}^* c_0^*)}{\partial z^*} = 0$$
$$\frac{\partial n_1^*}{\partial t^*} - c_1^* + \beta n_1^* = 0 \quad (26)$$

ε^2:

$$\frac{\partial c_2^*}{\partial t} + \frac{\partial c_2^*}{\partial z} + \frac{\partial n_2^*}{\partial t} + \frac{\partial(\tilde{u}^* c_1^*)}{\partial z} = 0$$
$$\frac{\partial n_2^*}{\partial t^*} - c_2^* + \beta n_2^* + c_1^* n_1^* = 0 \quad (27)$$

For simplicity and emphasis, here, we concentrate on the first-order accurate (zeroth-order) equations, since we feel these represent the simplest engineering approximation that captures the essence of the problem. We will later show in Part 2 of this two-paper series that predictions from these equations agree well with measurements of key ITP-AC parameters under our experimental conditions.[13] For interested readers, in section SI 1 in the Supporting Information, we discuss the more-accurate second- and third-order accurate formulations of our problem.

Initially, the affinity region is free from target, which supplies the initial condition $c(z,0) = 0$, $n(z,0) = 0$ (see Figure 1b). We model the Gaussian profile of the ITP focused target entering the affinity region as a time-varying boundary condition on the affinity region,

$$c(0, t) = a \exp\left[-\left(\frac{ut - 3\sigma}{\sqrt{2}\,\sigma}\right)^2\right] \quad (28)$$

representing a Gaussian distribution with maximum concentration a and standard deviation σ traveling at ITP velocity u (Figure 1b). We chose arbitrarily that, at $t = 0$, the Gaussian's maximum is 3σ to the left of the start of the affinity region and therefore just beginning to interact with the affinity region (Figure 1b). We then cast the initial and boundary conditions in the following nondimensionalized form:

$$c^*(z^*, 0) = n^*(z^*, 0) = 0 \quad (29)$$

$$c^*(0, t^*) = \frac{a}{N} \exp\left[-\left(\frac{ut^*}{k_1 N\sqrt{2}\,\sigma} - \frac{3}{\sqrt{2}}\right)^2\right] \quad (30)$$

We further introduce the following nondimensional parameters,

$$\alpha = \frac{a\sqrt{2\pi}}{N}$$
$$Da = \frac{\sigma k_1 N}{u} \quad (31)$$

and rewrite the boundary condition as

$$c^*(0, t^*) = \left(\frac{\alpha}{\sqrt{2\pi}}\right) \exp\left[\frac{-(t^*/Da - 3)^2}{2}\right] \quad (32)$$

Here, α represents the peak concentration of the target in the Gaussian distribution scaled by the initial probe concentration N. The Damkohler number (Da), as usual, describes the characteristic ratio between an electrophoretic (advection) time scale σ/u and the time scale of reaction $1/(k_1 N)$. Da is also usefully interpreted as a characteristic width of the Gaussian distribution scaled by advection-reaction length scale $u/(k_1 N)$. The product αDa is the total amount of target in the Gaussian distribution scaled by u/k_1 and, as we will show later, determines whether the affinity region locally saturates. We perform a straightforward expansion of the boundary and initial conditions (eqs 29 and 32), similar to that for eqs 23 and 24, and obtain

$$\varepsilon^0:\ c_0^*(z^*, 0) = n_0^*(z^*, 0) = 0$$
$$c_0^*(0, t^*) = \frac{\alpha}{\sqrt{2\pi}} \exp\left[-\frac{(t^*/Da - 3)^2}{2}\right]$$
$$\varepsilon^1:\ c_1^*(z^*, 0) = n_1^*(z^*, 0) = c_1^*(0, t^*) = 0$$
$$\varepsilon^2:\ c_2^*(z^*, 0) = n_2^*(z^*, 0) = c_2^*(0, t^*) = 0 \quad (33)$$

Therefore, eqs 25−27 and the initial and boundary conditions described in eq 33 constitute a well-posed, simplified description of our problem. Below, we present solutions to these equations, identify key figures of merit, and discuss a series of limiting regimes of practical interest to the experimentalist.

RESULTS AND DISCUSSION

Analytical Solution for Bound- and Free-Target Concentration. We analytically solved eqs 25 and demonstrate a solution method for eqs 26 and 27. Our approach is similar to that of Thomas,[22] but, here, subject to our boundary and initial conditions (eq 33), including our heuristic description of ITP zone shape and propagation. Briefly, we transformed eqs 25, 26, and 27 into a coordinate system moving with the ITP velocity. Then, we converted the result into a potential function form that collapses the two equations into a single equation. We then solved the resulting equation using Laplace transforms. We provide the full solution in section SI 1 in the Supporting Information. We obtained the following first-order accurate equations for the nondimensionalized bound target concentration,

$$n^* = 1 - \frac{1}{\varphi}\frac{\partial \varphi}{\partial z^*} + O(\varepsilon) \quad (34)$$

and for the free target concentration

$$c^* = \frac{1}{\varphi}\frac{\partial \varphi}{\partial y} - \beta + O(\varepsilon) \quad (35)$$

where

$$\varphi(z^*, y) = I_0(2\sqrt{\beta y z^*}) + \int_0^y \Lambda(y - y') I_0(2\sqrt{\beta y' z^*})\, dy' + \int_0^{z^*} \exp(z^* - z') I_0(2\sqrt{\beta y z'})\, dz' \quad (36)$$

dx.doi.org/10.1021/ac5011052 | Anal. Chem. 2014, 86, 6220−6228

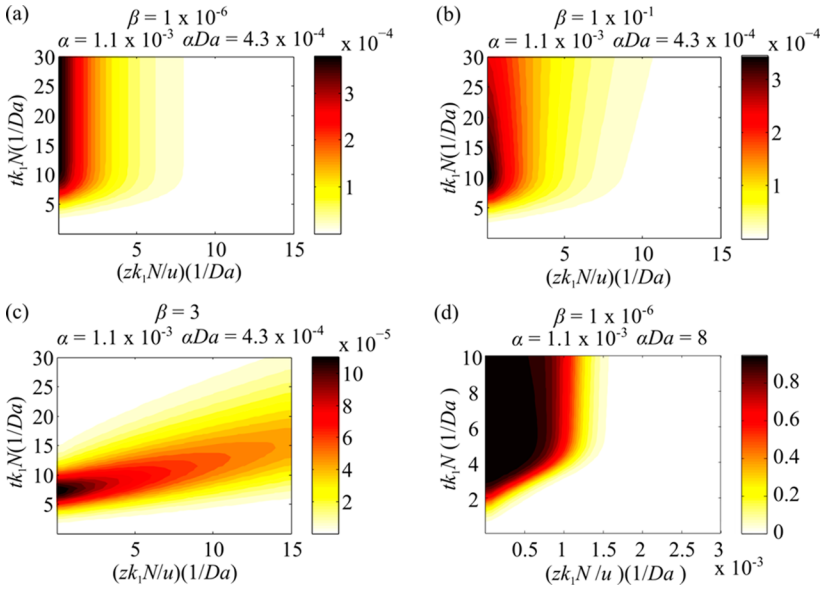

Figure 2. Model predictions of spatiotemporal dynamics of the bound target scaled by the initial probe concentration (n/N). The abscissa and ordinate can be interpreted as scaled axial distance and time, respectively. We show various values of nondimensionalized equilibrium dissociation constant β and saturation parameter αDa. Panels a, b, and c show the dependence of the spatiotemporal capture dynamics on β for $\alpha Da = 4.3 \times 10^{-4}$ and $\alpha = 1.1 \times 10^{-3}$ (nonsaturated regime, $\alpha Da < 1$). This set of αDa and α is similar to that in one of the experiments we will describe in Part 2 of this two-part series.[13] As β increases, the capture reaction becomes more reversible until $\beta \approx 3$, where the target is no longer effectively captured and streaks through the affinity region. Panel d shows spatiotemporal capture dynamics in a saturated regime ($\alpha Da > 1$). Here, the leading edge of the affinity region becomes saturated, shifting the spatiotemporal capture contours upward and to the right.

$$\Lambda(y) = \left(\frac{\alpha}{\sqrt{2\pi}} \exp\left[-\frac{(y/Da - 3)^2}{2}\right] + \beta\right) \times \exp\left\{y\beta + \frac{\alpha Da}{2}\left[\mathrm{erf}\left(\frac{y/Da - 3}{\sqrt{2}}\right) - \mathrm{erf}\left(\frac{-3}{\sqrt{2}}\right)\right]\right\} \quad (37)$$

$$y = t^* - z^* \quad (38)$$

Here, I_0 is the modified Bessel function of the first kind of zeroth order. For convenience, we evaluated numerical values of the solution using custom MATLAB scripts. We use these solutions to consider the effects of nondimensionalized target-probe dissociation constant, nondimensionalized target distribution width, and nondimensionalized peak distribution concentration on key affinity capture figures of merit: capture efficiency (n/N), capture length (p_z), and capture time (p_t). We then examine three important regimes of the solution: (a) $\alpha Da < 1$, (b) $Da \gg 1$, and (c) $\beta_{cn} \gg \beta_{target}$ (where the subscript "cn" refers to the contaminant).

Spatiotemporal Dynamics Predicted by Analytical Solution. *Effect of Nondimensionalized Equilibrium Dissociation Constant β.* In Figure 2, we plot representative solutions for the scaled bound-target concentration n/N versus scaled distance along the axis of the channel, and scaled times associated with a range of β from 10^{-6} to 3. These plots can be interpreted intuitively as spatiotemporal plots of the bound-target concentration (scalar) as a function of scaled distance and time in the abscissa and ordinate, respectively. In Figures 2a, 2b, and 2c, $\alpha Da = 4.3 \times 10^{-4}$ and $\alpha = 1.1 \times 10^{-3}$. In the regime of $\alpha Da < 1$, the affinity region is not locally saturated ($n/N < 1$). For relatively low β (e.g., 10^{-6}), the forward (affinity) reaction dominates and captured target remains bound. Here, as the target Gaussian peak enters the affinity region, the target binds and the concentration of the bound target n at the leading edge gradually increases with time (Figure 2a). At the same time, some of the target does not bind at the leading edge and is able to penetrate deeper into the affinity region and bind there. Even as this penetration proceeds, the target continues to bind near the leading edge. This creates the J-shaped bound-target concentration contours shown in Figure 2a. Under these conditions (as we will show in the section entitled "Control of Capture Length (p_z) below), 95% of the target is captured in ~2.8 advection-reaction length scales, providing an inherent nondimensional capture length. As β increases to $\sim 10^{-1}$, some of the target can desorb and readsorb during the effective capture time, and so the target can penetrate deeper into the affinity region (Figure 2b). For β on the order of unity and higher, the concept of a capture length becomes invalid, as the target migrates through the affinity region, continuously adsorbing and desorbing as it travels. For our characteristic values of Da and α, this continuous transport becomes very prominent at $\beta = 3$ (see Figure 2c). We hope to further study high-β, chromatographic-separation-type regimes in the future.

In the regime of $\alpha Da > 1$, the leading edge of the affinity region becomes saturated ($n/N = 1$). This forces the target to bypass the leading edge and penetrate deeper. In Figure 2d, we show the case where $\alpha Da = 8$, while α is still only 1.1×10^{-3}. We see that the effect of leading edge saturation is to establish a new effective leading edge for new captures. This new effective leading edge shifts up in time and rightward in the axial coordinate as free target penetrates and explores new regions of available sites (Figure 2d). The J-shaped profiles shift up and right accordingly. Under these conditions (as we will show in the section entitled "Control of Capture Length (p_z)" below), the length of the affinity region needed to capture 95% of the target depends mostly on the absolute amount of target and the capacity of the affinity region, N (and less sensitive to balances between reaction and advection times).

dx.doi.org/10.1021/ac5011052 | Anal. Chem. 2014, 86, 6220−6228

Control of Capture Length p_z. Figure 3 summarizes the major trends between advection, reaction, and capture length

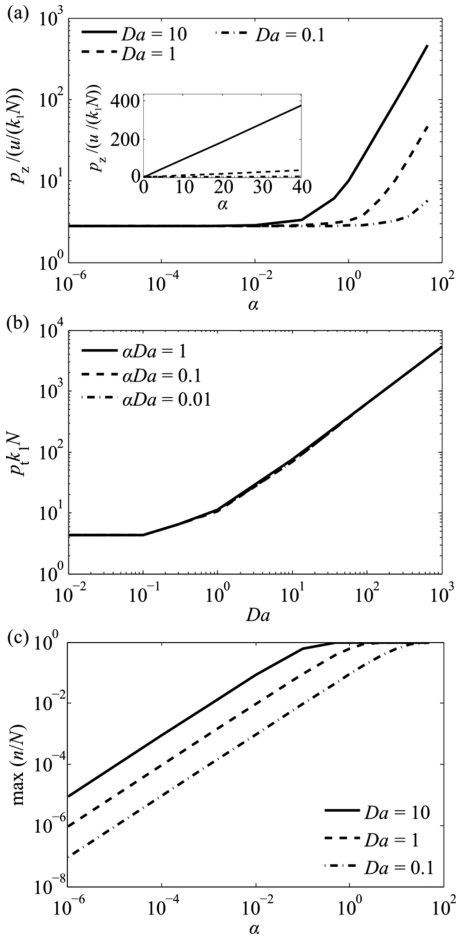

Figure 3. Model predictions for the (a) scaled capture length, (b) scaled capture time, and (c) maximum capture efficiency as a function of (a, c) scaled peak target concentration α and (b) scaled target distribution width Da for low β (plotted at $\beta = 10^{-4}$). Inset in (a) shows a linear plot of scaled capture length as a function of α from 0 to 40. In (a), when $\alpha Da < 1$ and so the affinity region is not locally saturated, capture length is only governed by the balance of reaction and advection, i.e., $u/(k_1N)$. Therefore, in this regime p_z^* is invariant of α or Da. When $\alpha Da > 1$ the affinity region becomes locally saturated and the length of saturated region governs the capture length. Since the length of locally saturated region is proportional to αDa, p_z^* is proportional to both α and Da. In (b), scaled capture time p_t^* is approximately 4.3 for $Da < 0.1$. For $Da > 1$, scaled capture time increases linearly with Da. Interestingly, the scaled capture time is independent of total scaled target amount, αDa (since the length scale of capture region is insensitive to capture amount provided ligand is not saturated, $\alpha Da \leq 1$). In (c) n/N increases linearly with α and Da for $\alpha Da < 1$ (i.e., when the affinity region is not saturated). For $\alpha Da > 1$ the affinity region becomes locally saturated and $n/N = 1$.

and time scales. We here formally define the dimensional capture length (p_z) as the physical length of the affinity column necessary to capture 95% of the target. Therefore, the inverse capture length is therefore a measure of efficiency of column utilization for columns of constant cross-sectional area. The parameter p_z is defined and useful only for small values of β, where the target is captured (versus transported through the region). We nondimensionalize this length by the advection-reaction length scale $u/(k_1N)$ and call this p_z^*.

Figure 3a shows major trends of p_z^*. Most importantly, we see that p_z^* solutions collapse to a constant value of 2.8 for $\alpha Da < 1$ (Figure 3a). α and Da represent the scaled target distribution height and width, respectively, so the product αDa represents the scaled total target amount. Only when $\alpha Da > 1$ does the target zone contain a sufficient amount of target to locally saturate the affinity region near the leading edge (Figure 2d). For $\alpha Da < 1$, the target amount is insufficient to locally saturate the affinity region. Therefore, for $\alpha Da < 1$, the capture length only depends on the balance of advection and reaction, i.e., $u/(k_1N)$. Hence, in this regime, p_z is proportional to $u/(k_1N)$. Thus, also p_z^* is independent of α or Da as long as the product $\alpha Da < 1$ (Figure 3a). For $\alpha Da > 1$, the affinity region becomes locally saturated and the length of the locally saturated region dominates the capture length. Also in this regime, the saturated length increases in direct proportion to the total amount of target and, therefore, p_z^* increases linearly with the product αDa (see Figure 3a).

Control of Capture Time p_t. We define a capture time (p_t) as the time necessary to capture 95% of the target. Similar to capture length, this time is defined only for small values of β, where the target is captured and does not appreciably desorb during the capture process. The capture time is proportional to the ITP-AC assay time for assays designed to capture nearly all of the target. We nondimensionalize this time by the reaction time scale $1/(k_1N)$ and call this parameter p_t^*. For the unsaturated regime of $\alpha Da \leq 1$, scaled capture time p_t^* depends only on scaled target distribution width Da and is insensitive to the total to the total amount of target αDa. Thus, we see that scaled capture times all collapse to a value of 4.3 for Da less than ~0.1 and for $\alpha Da \leq 1$ (Figure 3b). In this regime, the target distribution standard deviation is significantly less than the advection-reaction length scale and the target distribution effectively acts as a Dirac delta distribution. Consequently, the time scale for capture is governed solely by the reaction time scale, $1/(k_1N)$. In this regime, the absolute capture length p_z is still $\sim 2.8u/(k_1N)$, and the target's travel lasts $4.3/(k_1N)$. For $Da > 1$ (i.e., sufficiently wide scaled distributions), p_t^* increases linearly with Da (Figure 3b). The latter is simply because it takes proportionally more time for a wider distribution to completely enter the affinity region and be captured.

These observations lead us to the conclusion that there is little need to decrease the target distribution width below $\sim 0.1u/(k_1N)$. That is, the regime of $Da < 1$ is sufficient to remove dependence on the initial target distribution. As we shall show in Part 2 of this paper, such target distribution widths are readily achievable using ITP focusing.

In traditional AC, the target is introduced to an affinity column with spatial distributions, which are much wider and lower concentration than ITP achieves. ITP has been demonstrated to increase target concentration (and proportionately decrease target distribution width) up to 10^6-fold under ideal conditions,[23] and to order 10^4-fold for the case of nucleic acids from complex biological samples.[8] The trends discussed above therefore suggest that increases in concentration via ITP can translate to proportionally lower capture times and lower capture lengths. For example, consider that reaction times for wide distributions ($Da \gg 1$) benefit directly from any decrease in target zone width (c.f. Figure 3b). Furthermore, consider that, for a fixed assay time, ITP preconcentration enables much lower advection velocity u

dx.doi.org/10.1021/ac5011052 | Anal. Chem. 2014, 86, 6220−6228

and so proportionally lower capture lengths, thus maximizing column utilization.

Control of Capture Efficiency (n/N). We define the capture efficiency as the concentration of target captured over the initial concentration of probe, n/N) (a maximum of unity). The trends of capture efficiency are summarized in Figure 3c. For small β (i.e., approximately irreversible reactions), the highest value of n/N occurs at the leading edge of the affinity region, where the affinity sites see the largest amount of target. For small β and $\alpha Da < 1$ (locally not saturated), the highest n/N (at the leading edge) is proportional to the total amount of target that enters the affinity region. Hence, the highest value of n/N increases linearly with αDa until αDa reaches unity. For $\alpha Da \geq 1$, the capture zone saturates near the leading edge, yielding a n/N value near unity.

In Figure 4, we summarize the effect of β on capture efficiency as a function of the scaled target distribution width

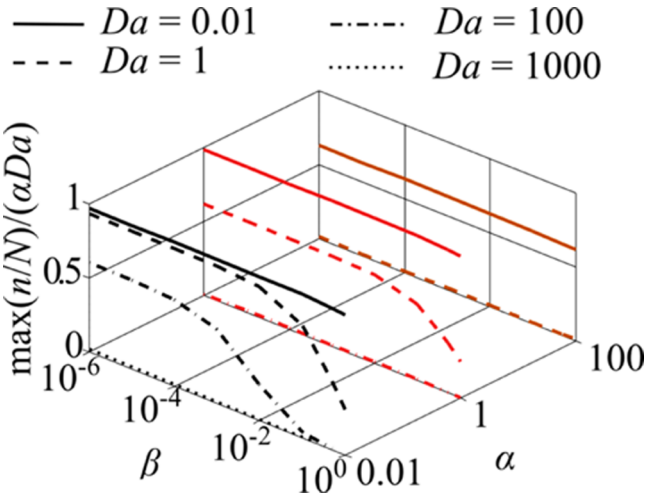

Figure 4. max(n/N) scaled by αDa for values of β between 10^{-6} and 1, Da between 0.01 and 1000, and α between 0.01 and 100. As β increases the reverse reaction (dissociation) becomes more prominent until no effective binding occurs and the target streaks through the affinity region. Capture efficiency n/N always decreases with increasing β, and this effect becomes more pronounced with increasing Da and α. Therefore, decreasing Da (e.g., by preconcentrating the target with ITP) allows one to achieve larger capture efficiencies for a given dissociation constant.

Da, and scaled distribution peak concentration α. Here, we plot the maximum value of n/N, max(n/N), normalized by the scaled total target amount αDa. Overall, as β increases, the capture efficiency decreases (Figure 4), because of increasing reversibility of the capture. This increased adsorption/desorption of the target "smears" the target over a larger area of the affinity region (see Figure 2c). As the affinity region becomes more locally overloaded (i.e., as α approaches and becomes greater than unity), the affinity region locally cannot capture the entire target distribution, necessitating the target distribution to migrate some distance. This widens the target distribution. When β is relatively large (e.g., 10^{-3}), desorption is prominent and so the wide bound-target distribution is smeared over longer distances. Therefore, increasing α decreases capture efficiency in this regime. Similarly, when desorption is prominent, the wider the target distribution entering the affinity region (i.e., the larger the Da), the more smeared the distribution becomes. Hence, capture efficiency decreases with increasing Da. Thus, decreasing Da (such as with strong ITP preconcentration) enables efficient capture of targets with larger dissociation constants.

Limiting Regimes of ITP-Aided Capture Dynamics. We summarize several limiting regimes of immediate interest to the experimentalist, as well as associated closed-form (algebraic) solutions for the associated figures of merit.

Capture Length in the Low αDa Regime. The low αDa regime is associated with an affinity region that is not locally saturated; thus, the concentration of bound target remains proportional to the total target amount (see the section entitled "Control of Capture Efficiency (n/N)"). Therefore, this is an important regime for analytical quantification of target using ITP-AC. In this regime, $p_z^* \approx 2.8$, and this value is invariant of αDa, as shown in Figure 3a. Therefore, we can express the dimensional capture length as simply

$$p_z \approx \frac{2.8u}{k_1 N} \tag{39}$$

This relation predicts the capture length to within 1% for $\alpha Da < 0.1$ and to within 20% for $\alpha Da < 1$. This relationship also allows a simple way to measure the forward rate constant k_1 from a measurement of p_z, as u is set by setting running current for ITP (and measured by simple observations), and N is easily measured (see the section entitled "Measurement of ITP-AC Parameters" of Part 2 of this two-part series[13]).

Capture Time in the High Da Regime. In the high Da regime, the scaled target distribution width becomes much larger than the advection-reaction length scale and, therefore, much larger than the capture length (albeit for nonsaturated conditions, so that $\alpha Da < 1$). In this regime, the capture time is solely determined by the time for the ITP zone to enter the affinity region and we can write (c.f. Figure 2b)

$$p_t \approx \frac{5.4\sigma}{u} \tag{40}$$

This relationship predicts the capture time to within 13% for $Da > 100$ and $\alpha Da \leq 1$, and to within 24% for $Da > 10$ and $\alpha Da \leq 1$.

Separation Resolution of ITP-AC. In ideal ITP-aided capture, $\beta_{cn} \gg \beta_{target}$ (where the subscript "cn" refers to contaminant). This creates the opportunity to capture target (in time p_t) while allowing contaminants to migrate through the column. Here, we consider a regime where the target is completely captured (e.g., $\beta < 10^{-6}$) while the contaminant species remains focused in ITP and migrates at the ITP velocity. Following the common definition of resolution given by Giddings,[24] and setting the width of captured target distribution as p_z and approximating the width of the ITP peak as per the classic theory of MacInnes and Longsworth,[21,25] we can obtain the scaling for resolution for ITP-AC as

$$R_{\text{ITP-AC}} \approx \frac{ut}{\frac{u}{k_1 N} p_z^* + \frac{1}{u}\left(\frac{\mu_{\text{L in LE}}\mu_{\text{T in TE}}}{\mu_{\text{L in LE}} - \mu_{\text{T in TE}}}\right)\frac{k_B T}{e}} \tag{41}$$

Here, k_B is the Boltzmann's constant, T is the absolute temperature, e is the electron charge, and $\mu_{\text{L in LE}}$ and $\mu_{\text{T in LE}}$ are the mobilities of the LE ion in the LE and the TE ion in the TE, respectively. We observe that the resolution for ITP-AC scales as proportional with time t. This is in sharp contrast to the resolution of traditional electrophoresis or of AC which scale as $t^{1/2}$.[26] We provide more details regarding the derivation

dx.doi.org/10.1021/ac5011052 | Anal. Chem. 2014, 86, 6220−6228

and analysis of resolution of ITP-AC processes in the section SI 2 in the Supporting Information.

CONCLUSIONS

We have developed an analytical model for the spatiotemporal dynamics of isotachophoresis coupling with affinity chromatography (ITP-AC). We investigated the coupled effects of target distribution width, distribution intensity, application velocity, forward and reverse reaction constants, and probe concentration on necessary affinity capture length, assay time, and capture efficiency. We collapsed these six independent variables to three nondimensionalized parameters (α, β, and Da) and identified key limiting regimes in the problem.

We showed that scaled capture length (length necessary to capture 95% of the target scaled by the advection-reaction length scale) approaches a constant value of ∼2.8 for the regime where the scaled total target amount, αDa, is less than approximately unity. (α and Da represent the scaled target distribution height and width, respectively.) In this regime, the affinity region is not locally saturated and the maximum concentration of bound target is proportional to the total amount of target in the distribution. Therefore, this regime provides a simple way to quantify the total amount of target. For αDa values greater than unity, the affinity region is locally saturated and the scaled capture length increases linearly with αDa. The saturation effectively shifts the leading edge of the capture zone progressively downstream until new capture sites are available. We also showed how increasing the nondimensionalized equilibrium dissociation constant β decreases the capture efficiency n/N. The strength of this effect increases as both α and Da increase.

We showed that the scaled capture time (time necessary to capture 95% of the target, scaled by the reaction time scale) asymptotes to ∼4.3 for $Da < 0.1$ and $\alpha Da \leq 1$. In this relevant regime, the target distribution acts a Dirac delta function. For Da greater than approximately unity, the scaled capture time increases linearly with Da, indicating that the capture of wide target distributions in this regime is simply limited by the time for them to enter the affinity column. By focusing the target into a narrow distribution, as is achieved with ITP, we decrease Da and therefore decrease the overall assay time. Furthermore, assay time is set by the time required to advect the target into the affinity region, which scales as the target distribution width divided by the target velocity (σ/u). Therefore, for a fixed assay time, preconcentration yields a proportionally lower capture length p_z, and improved column utilization.

Lastly, we showed that the resolution of the most common mode, ITP-AC purification, should scale proportionally with time. Experimental validations of our model and a demonstration of ITP-AC purification of a target from a 10 000-fold more-abundant contaminant will be presented in Part 2 of this two-paper series.[13]

ASSOCIATED CONTENT

Supporting Information

This material is available free of charge via the Internet at http://pubs.acs.org.

AUTHOR INFORMATION

Corresponding Author

*Tel.: 650-723-5689. Fax: 650-723-7657. E-mail: juan.santiago@stanford.edu.

Notes

The authors declare no competing financial interest.

ACKNOWLEDGMENTS

We gratefully acknowledge support from the National Institutes of Health Progenitor Cell Biology Consortium (No. 5U01HL099997, subcontract SR00002307). We also gratefully acknowledge support from the National Science Foundation under contract number CBET-1159092 and for a Graduate Research Fellowship for Viktor Shkolnikov.

REFERENCES

(1) Hage, D. S. *Handbook of Affinity Chromatography*; CRC Press: Boca Raton, FL, 2006.
(2) Hage, D. S. *Clin. Chem.* **1999**, *45*, 593−615.
(3) Mallik, R.; Hage, D. S. *J. Sep. Sci.* **2006**, *29*, 1686−1704.
(4) Pfaunmiller, E. L.; Paulemond, M. L.; Dupper, C. M.; Hage, D. S. *Anal. Bioanal. Chem.* **2013**, *405*, 2133−2145.
(5) Levenspiel, O. *Chemical Reaction Engineering*, 3rd Edition; John Wiley & Sons: New York, 1999.
(6) Everaerts, F. M.; Beckers, J. L.; Verheggen, T. P. E. M. *Isotachophoresis: Theory, Instrumentation, and Applications*; Elsevier: Amsterdam, 1976.
(7) Bocek, P. *Analytical Isotachophoresis*; VCH: Weinheim, Germany, 1987.
(8) Rogacs, A.; Marshall, L. A.; Santiago, J. G. *J. Chromatogr. A* **2014**, *1335*, 105−120.
(9) Bercovici, M.; Han, C. M.; Liao, J. C.; Santiago, J. G. *Proc. Natl. Acad. Sci. U.S.A.* **2012**, *109*, 11127−11132.
(10) Garcia-Schwarz, G.; Santiago, J. G. *Anal. Chem.* **2012**, *84*, 6366−6369.
(11) Garcia-Schwarz, G.; Santiago, J. G. *Angew. Chem.* **2013**, *125*, 11748−11751.
(12) Karsenty, M.; Rubin, S.; Bercovici, M. *Anal. Chem.* **2014**, *86*, 3028−3036.
(13) Shkolnikov, V.; Santiago, J. G. *Anal. Chem.* **2014**, DOI: 10.1021/ac5011074).
(14) Garcia-Schwarz, G.; Rogacs, A.; Bahga, S. S.; Santiago, J. G. *J. Visualized Exp.* **2012**, *61*, e3890 (DOI: 10.3791/3890).
(15) Khurana, T. K.; Santiago, J. G. *Anal. Chem.* **2008**, *80*, 6300−6307.
(16) Garcia-Schwarz, G.; Bercovici, M.; Marshall, L. A.; Santiago, J. G. *J. Fluid Mech.* **2011**, *679*, 455−475.
(17) Shim, J.; Dutta, P.; Ivory, C. F. *Numer. Heat Transfer, Part A* **2007**, *52*, 441−461.
(18) Dullien, F. A. L. *Porous Media: Fluid Transport and Pore Structure*, 2nd Edition; Academic Press: New York, 1991.
(19) Incropera, F. P.; DeWitt, D. P. *Fundamentals of Heat and Mass Transfer*; John Wiley & Sons: New York, 1996.
(20) Stellwagen, E.; Stellwagen, N. C. *Electrophoresis* **2002**, *23*, 2794−2803.
(21) MacInnes, D. A.; Longsworth, L. G. *Chem. Rev.* **1932**, *9*, 171−230.
(22) Thomas, H. C. *J. Am. Chem. Soc.* **1944**, *66*, 1664−1666.
(23) Jung, B.; Bharadwaj, R.; Santiago, J. G. *Anal. Chem.* **2006**, *78*, 2319−2327.
(24) Giddings, J. C. *Sep. Sci. Technol.* **1969**, *4*, 181−189.
(25) Shkolnikov, V.; Bahga, S. S.; Santiago, J. G. *Phys. Chem. Chem. Phys.* **2012**, *14*, 11534−11545.
(26) Landers, J. P. *Handbook of Capillary Electrophoresis*; CRC Press: Boca Raton, FL, 1997.